



Contents lists available at ScienceDirect

## Spectrochimica Acta Part A: Molecular and Biomolecular Spectroscopy

journal homepage: [www.elsevier.com/locate/saa](http://www.elsevier.com/locate/saa)

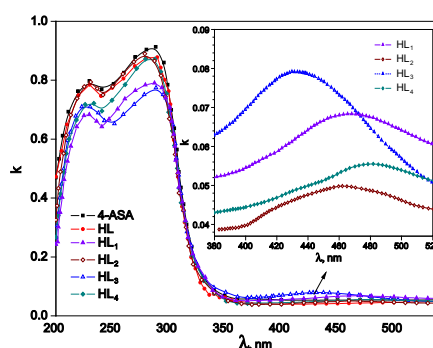
## Optical and thermal properties of azo derivatives of salicylic acid thin films

M.M. Ghoneim<sup>a</sup>, N.A. El-Ghamaz<sup>b</sup>, A.Z. El-Sonbati<sup>c,\*</sup>, M.A. Diab<sup>c</sup>, A.A. El-Bindary<sup>c</sup>, L.S. Serag<sup>c,1</sup><sup>a</sup> Chemistry Department, Faculty of Science, Tanta University, Tanta, Egypt<sup>b</sup> Physics Department, Faculty of Science, Damietta University, Damietta, Egypt<sup>c</sup> Chemistry Department, Faculty of Science, Damietta University, Damietta, Egypt

## HIGHLIGHTS

- We examine changes in optical properties for 4-ASA and its derivatives.
- All the thermal parameters are affected by amidation and diazotization processes.
- The XRD pattern of the powder and thin film forms are polycrystalline and amorphous, respectively.
- The optical transitions are found to be indirect allowed.
- Diazotization remarkably enhances the photoluminescence spectra.

## GRAPHICAL ABSTRACT

Spectral behavior of absorption index,  $k$ , for 4-ASA, HL and HL<sub>*n*</sub> thin films.

## ARTICLE INFO

## Article history:

Received 27 May 2014

Received in revised form 28 June 2014

Accepted 24 August 2014

Available online 18 September 2014

## Keywords:

Azo salicylic acid

Spin coating

Fluorescence

X-ray diffraction

Thermal and optical properties of thin films

## ABSTRACT

*N*-acryloyl-4-aminosalicylic acid (4-AMSA), monomer (HL) and 5-(4'-alkyl phenylazo)-*N*-acryloyl-4-aminosalicylic acid (HL<sub>*n*</sub>) are synthesized and characterized with various physico-chemical techniques. Thin films of 5-(4'-alkyl phenylazo)-*N*-acryloyl-4-aminosalicylic acid (HL<sub>*n*</sub>) are prepared by spin coating technique. The X-ray diffraction (XRD) patterns of 4-aminosalicylic acid (4-ASA) and its derivatives are investigated in powder and thin film forms. Thermal properties of the compounds are investigated by thermogravimetric analysis (TGA). The optical properties of the compounds are investigated in the wavelength range (200–2500 nm) for 4-ASA, HL and HL<sub>*n*</sub>. The values of fundamental energy gap ( $E_g$ ) are in the range 3.60–3.69 eV for all compounds and the type of optical transition is found to be indirect allowed. The onset energy gap  $E_g^*$  appeared only for azodye compounds is found to be in the range 0.95–1.55 eV depending on the substituent function groups. The refractive index,  $n$ , shows a normal dispersion in the wavelength range 650–2500 nm, while shows anomalous dispersion in the wavelength range 200–650 nm. The dispersion parameters  $\epsilon_\infty$ ,  $\epsilon_L$ ,  $E_d$ ,  $E_o$  and  $N/m^*$  are calculated. The photoluminescence phenomena (PL) appear for thin films of 4-ASA and its derivatives show three main emission transitions.

© 2014 Elsevier B.V. All rights reserved.

## Introduction

Aromatic azo compounds constitute a very important class of organic compounds because of their widespread applications in

\* Corresponding author. Tel.: +20 1060081581; fax: +20 572403868.

E-mail address: [elsonbatsch@yahoo.com](mailto:elsonbatsch@yahoo.com) (A.Z. El-Sonbati).<sup>1</sup> Abstracted from her M.Sc.

many areas of organic dyes [1], indicators [2], radical reaction initiators [3,4], and therapeutic and drug delivery agents [5–7]. They are also important units in the area of nonlinear optics [8], optical storage media [9], chemosensors [10], photochemical switches [11] and electronic devices [12].

Salicylic acid and its derivatives are widely used in many applications such as, pharmaceutical industry [13,14], skin-care products [15], food antiseptic, pesticide, cleanser textiles [16], analgesic, antipyretic, anti-inflammatory bowel diseases (IBD) and anti-tuberculosis drug [17,18].

4-Aminosalicylic acid (4-ASA) was conjugated with various carrier molecules to get new azo derivatives of 4-ASA [17,18]. Azo salicylic acid derivatives are presented remarkable anti-inflammatory activity and antioxidant activity which attributed to the co-antioxidant effects of 4-ASA and substituted phenol with higher reducibility, according to the superoxide dismutase (SOD) activity [18].

4-Aminosalicylic acid has been successfully intercalated into zinc layered hydroxide (ZLH) using zinc oxide suspension by Saifullah et al. [19]. The X-ray diffraction patterns and FTIR analyses indicated that the molecule has been intercalated into the ZLH interlayer space with an average basal spacing of 24 Å. Furthermore, they discussed that TG curve of 4-ASA showed two stages; the first one in the temperature range 101–150 °C was attributed to dehydration. The second stage in the temperature range 150–235 °C was related to combustion of 4-ASA. The thermal behavior has been changed with intercalated 4-ASA anions (decomposition occurs at 227 °C) compared to 4-ASA anions. 4-ASA-ZLH has been remarkably enhanced thermal stability. Rotich et al. [20] discussed the thermal properties of 4-ASA, which gives a two stage mass loss with discontinuity after about 30% mass loss at close to the melting point (130 °C) of 4-ASA. The weight loss at discontinuity close to calculated CO<sub>2</sub> content but the evolution of CO<sub>2</sub> occurs during the latter stage of the TG curve. The corresponding enthalpy ( $\Delta H_{\text{vap}}$ ) for the two stages, in the temperature region 130–150 °C and 150–180 °C, have been calculated and found to be 250 ± 40 and 50 ± 5 kJ mol<sup>-1</sup>, respectively.

A series of aromatic molecules which display strong internal hydrogen bonding has been studied as regards the existence of phototropic tautomerism both in the ground and excited state [21–23]. Transition energies of all tautomers for the allowed  $\pi-\pi^*$  transition shows that keto-hydrazone tautomers absorbed at longer wavelengths when compared with enol-azo tautomers. Larger Stokes shifts can be ascribed to excited state intramolecular proton transfer (ESIPT) processes, whereas smaller Stokes shifts can be regarded as belonging to normal emission bands arising from the primary excited structure [21,22]. A proton-transferring for 1,4-bis-*p*-sulfonylazo-2,3 dihydroxy naphthalene (SADN), and its possible binuclear copper(II) complexes have been studied in aqueous solution [23]. The results provided evidence that SADN undergoes both single and double excited state intramolecular proton transfer (ESIPT) phenomena.

Three azopyrrole compounds have been synthesized and their structures have been determined by single crystal X-ray diffraction, <sup>1</sup>H NMR and UV-Vis spectra by Chen and Yin [24]. They reported that it is cooperative intramolecular hydrogen bonds that influence the azopyrrole tautomerisation from the azo to the hydrazone form, only if adding a hydrogen bond acceptor on the benzene ring to the ortho-position of azo linkage. It is also necessary to add a hydrogen bond donor to the pyrrole side and build two cooperative intramolecular hydrogen bonds.

Fluorescence spectra of rare earth complex polystyrene with side chain bonded salicylic acid (SA), SAPS-Eu(III), have been investigated [25]. There were two absorption peaks at 273 and 315 nm, which attributed to  $\pi-\pi^*$  electron transition of benzene ring of polystyrene backbone and the carboxyl group of SA ligand. The excitation spectrum of SAPS-Eu(III) was obtained at 618 nm

when ( $\lambda_{\text{ex}} = 346 \text{ nm}$ ). The increase of SA coordinating to Eu<sup>3+</sup> ion, leading to the enhancement of fluorescence emission intensity of the complex SAPS-Eu(III).

Konjac glucomannan (KGM) has been interacted with 4-aminosalicylic acid (4-ASA) to produce 4-ASA-KGM blends [26]. The fluorescence spectra of both 4-ASA and 4-ASA-KGM blends exhibited an identical emission spectra at 390 nm. It was found that the presence of KGM cause the fluorescence quench and the emission intensity increased proportionally with increasing of 4-ASA concentration in aqueous solutions. Joshi et al. [27] reported that the amino substitution at 4-position does not lead to dual emission, unlike 5-aminosalicylic acid (5-ASA). Contrary, Suyal et al. [28] reported that 4-ASA fluorescence emission shows dual emission in poly (vinyl alcohol) (PVA), poly (methyl methacrylate) (PMMA) and cellulose acetate (CA). They also reported that, 4-ASA is present as two rotomers (*P* and *R*) and rotomer *P* is more stable than *R*-due to strong intramolecular hydrogen bond. Rotomer *R* cannot undergo ESTPT and has normal fluorescence band. Dual emission was observed in the polymers. They attributed the emission peaks at longer wavelength to ESIPT, while the band at 330 nm is due to those rotomer which cannot undergo ESIPT.

Due to the importance of azo compounds and salicylic acid derivatives and their applications, the present work aims to investigate the dispersion, absorption and emission spectra of 4-ASA and its azo derivatives to produce new materials having promising technological applications such as nonlinear optics devices, solar cells and light emitting display LED.

## Experimental

### Materials

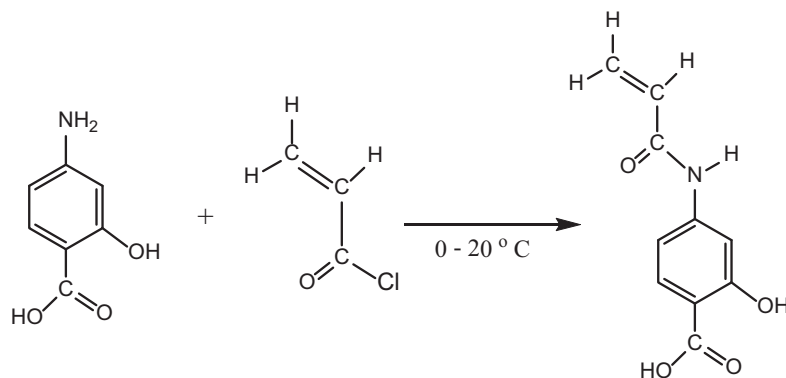
Acryloyl chloride (AC) (Aldrich Chemical Co., Inc.) was used without further purification. It was stored below –18 °C in a tightly glass-stoppered flask. Aniline and 4-*R*-aniline (R=OCH<sub>3</sub>, CH<sub>3</sub>, Cl and NO<sub>2</sub>) (Aldrich Chemical Co., Inc.) also was used without further purification. 4-Aminosalicylic acid (Aldrich chemical Co., Inc.) was purified by recrystallization from hot ethanol and filtering. All other chemicals and solvents were purified by standard procedures.

### Synthesis of *N*-acryloyl-4-aminosalicylic acid (HL)

*N*-Acryloyl-4-aminosalicylic acid – (4-AMSA) – monomer (HL) was performed by the amidation reaction of equimolar amounts of AC and 4-aminosalicylic acid in dry benzene until the evolution of hydrogen chloride caused forming a gray powder of HL monomer [29] as shown in Scheme 1.

### Synthesis of 5-(4'-alkyl phenylazo)-*N*-acryloyl-4-aminosalicylic acid (HL<sub>*n*</sub>)

5-(4'-Alkyl phenylazo)-*N*-acryloyl-4-aminosalicylic acid (HL<sub>*n*</sub>) were prepared in our laboratories by diazotization reaction. In a typical preparation [30–34], 25 ml of distilled water containing 0.01 mol hydrochloric acid are added to aniline (0.01 mol) or *p*-derivatives. To the resulting mixture stirred and cooled to 0 °C, a solution of 0.01 mol sodium nitrite in 20 ml of water was added dropwise. The formed diazonium chloride is consecutively coupled with an alkaline solution of 0.01 mol *N*-acryloyl-4-aminosalicylic acid, in 10 ml of pyridine. The colored precipitate, which formed immediately, is filtered through sintered glass crucible, washed several times with water and ether. The crude products was purified by recrystallization from hot mixture of ethanol and water then dried in vacuum desiccator over P<sub>2</sub>O<sub>5</sub>.



**Scheme 1.** The formation mechanism of *N*-acryloyl-4-aminosalicylic acid (HL).

The resulting formed ligands are:

- 5-(4'-methoxyphenylazo)-*N*-acryloyl-4-aminosalicylic acid (HL<sub>1</sub>),
- 5-(4'-phenylazo)-*N*-acryloyl-4-aminosalicylic acid (HL<sub>2</sub>),
- 5-(4'-chlorophenylazo)-*N*-acryloyl-4-aminosalicylic acid (HL<sub>3</sub>),
- 5-(4'-nitrophenylazo)-*N*-acryloyl-4-aminosalicylic acid (HL<sub>4</sub>),

which are shown in [Scheme 2](#).

#### Preparation of thin films

Thin films of 4-ASA, HL and HL<sub>*n*</sub> with good homogeneity are prepared by spin coating technique [35] onto optical flat and well-cleaned glass substrates. The coating system is locally constructed in our laboratory. The speed of spin coating machine was adjusted to 2800 rps. 0.001 mol of all compounds are dissolved in ethanol and dropped onto the rotating substrate to form thin films at room temperature.

#### Analysis techniques

Elemental microanalyses of the separated compounds for C, H, and N were determined on Automatic Analyzer CHNS Vario ELIII, Germany. The analyses were repeated twice to check the accuracy of the analyzed data. The FTIR spectra are recorded as KBr disks using Perkin-Elmer 1340 spectrophotometer. X-ray diffraction patterns of the powder and the thin film forms, are recorded on X-ray

diffractometer (GNR APD-2000 PRO) with CuK $\alpha$ -radiation ( $\lambda = 1.540598 \text{ \AA}$ ) in the range of diffraction angle ( $2\theta^\circ = 4\text{--}70^\circ$ ). The applied voltage and the tube current are 40 KV and 30 mA, respectively. Measurements of transmittance,  $T(\lambda)$ , and reflectance,  $R(\lambda)$ , of the thin film samples are carried out at room temperature and at normal incidence of light in the wavelength range 200–2500 nm in steps of 2 nm using a double-beam spectrophotometer (JASCO model V-570-UV/Vis/NIR). Thermal properties were investigated using Simultaneous Thermal Analyzer (TGA) STA 6000 with a scan rate 10 °C/min in air atmosphere from ambient temperatures to 600 °C. Photoluminescence spectra are recorded on Fluorimeter spectrophotometer (model 6285, for excitation and emission spectra, 200–700 nm).

#### Determination of optical constants of thin films

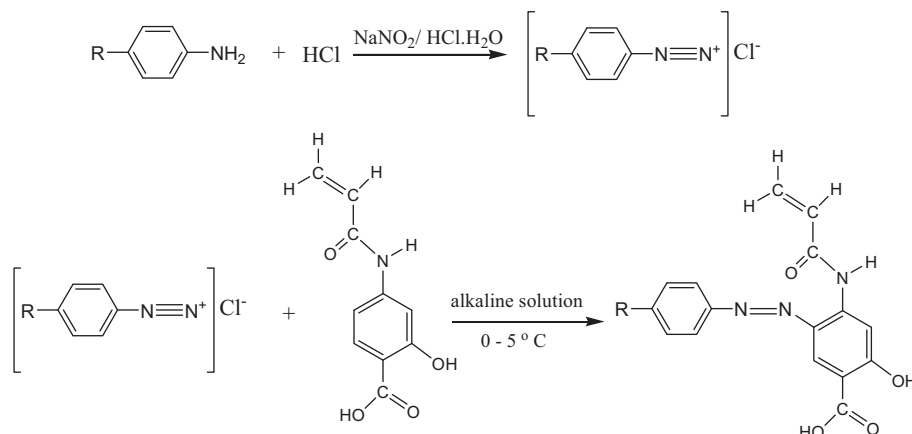
The absolute values of transmittance,  $T(\lambda)$ , and reflectance,  $R(\lambda)$ , which are used to calculate the optical constants are calculated according to the relation [36]:

$$T(\lambda) = \left( \frac{I_{fr}}{I_g} \right) (1 - R_g), \quad (1)$$

and

$$R(\lambda) = \left( \frac{I_{fr}}{I_{Al}} \right) R_{Al} \left[ \left( 1 + \left( 1 - (R_g)^2 \right) \right) \right] - TR_g, \quad (2)$$

where  $I_{fr}$  and  $I_g$  are the intensities of light passing through film-glass system and reference glass substrate, respectively.  $I_{fr}$  and  $I_{Al}$  are the intensities of the light reflected from the sample and that



**Scheme 2.** The formation mechanism of 5-(4'-alkyl phenyl azo)-*N*-acryloyl-4-aminosalicylic acid (HL<sub>*n*</sub>); R=OCH<sub>3</sub> (*n* = 1), H (*n* = 2), Cl (*n* = 3) and NO<sub>2</sub> (*n* = 4).

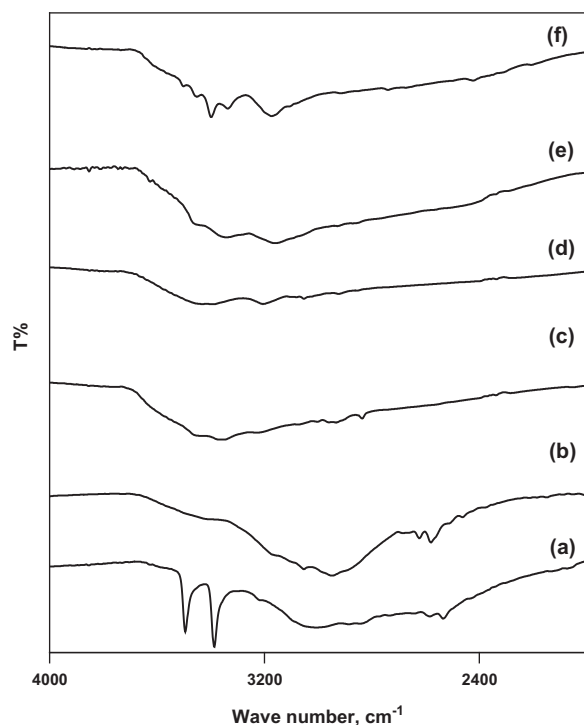


Fig. 1. The IR spectrum of; (a) 4-ASA, (b) HL, (c) HL<sub>1</sub>, (d) HL<sub>2</sub>, (e) HL<sub>3</sub> and (f) HL<sub>4</sub>.

from the reference mirror, respectively.  $R_{Al}$  is the reflectance of Al-mirror and  $R_g$  is the reflectance of the glass.

The refractive index,  $n$ , is an important parameter for optical materials design and it includes valuable information for optical materials with higher efficiency. The complex refractive index ( $n^*$ ) can be expressed as:

$$n^* = n - ik, \quad (3)$$

where  $n$  is the real part of the refractive index and  $k$  is the absorption index. The values of absorption coefficient,  $\alpha$ , ( $=4\pi k/\lambda$ ) of thin films can be calculated from the  $T(\lambda)$  and  $R(\lambda)$  according to the relation [37–39]:

$$\alpha = \left(\frac{1}{d}\right) \ln \left[ \frac{(1-R)^2}{2T} + \sqrt{\left(\frac{(1-R)^4}{4T^2} + R^2\right)} \right], \quad (4)$$

where  $\lambda$  is the wavelength of the incident light on the sample,  $d$  is the thickness of the film  $\approx$  (100) nm.

The refractive index,  $n$  of thin films is calculated according to the relation:

$$n = \frac{(1+R)}{(1-R)} + \sqrt{\left(\left(\frac{4R}{(1-R)^2}\right) - k^2\right)}, \quad (5)$$

Table 1  
The important IR spectra bands of 4-ASA, HL and its azo derivatives.

Compound	Assignment (cm <sup>-1</sup> )			
	$\nu(\text{NH}_2)$	$\nu(\text{OH Phenolic, Carboxylic and NH})$	$\nu(\text{C=O})$	$\nu(\text{N=N})$
4-ASA	3474, 3390	3006, 2889	1652	-
HL	-	3400, 3050, 2950	1679, 1612	-
HL <sub>1</sub>	-	3458, 3351, 3207	1614, 1604	1504
HL <sub>2</sub>	-	3440, 3388, 3205	1610, 1600	1504
HL <sub>3</sub>	-	3460, 3342, 3158	1627, 1585	1500
HL <sub>4</sub>	-	3397, 3338, 3174	1658, 1635	1509

## Results and discussion

### Characterization of ligands

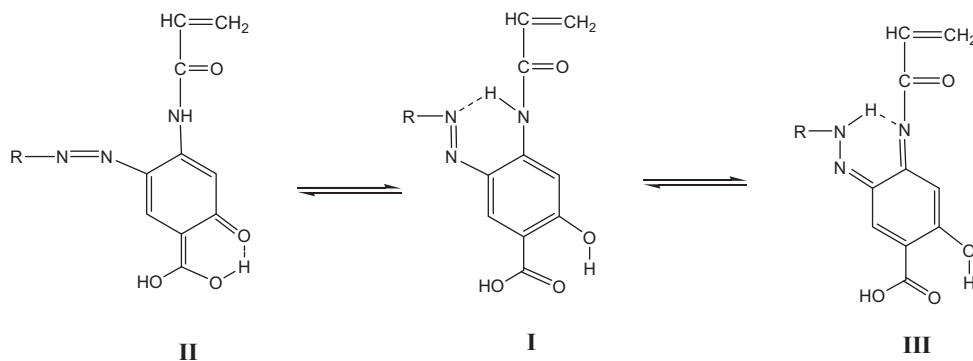
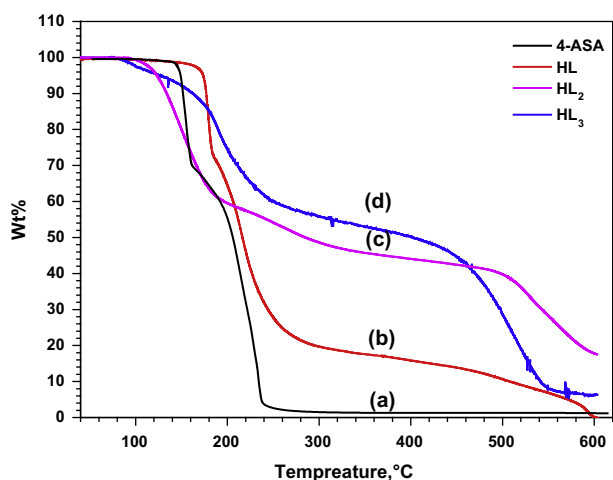
Microanalytical data are in good agreement with the stoichiometry of the proposed structures.

### FT-IR spectra

The Fourier transform infrared spectrum (FT-IR) of 4-ASA in comparison with its derivatives is presented in Fig. 1. The main absorption peaks are tabulated in Table 1. The IR spectrum for 4-ASA (Fig. 1(a)) shows NH<sub>2</sub> group absorption peaks at 3474 and 3390 cm<sup>-1</sup>. The OH stretching broad bands of the phenolic and carboxylic acid groups at 3006 and 2889 cm<sup>-1</sup>, respectively. This broadening is an evidence for the presence of weak hydrogen bond between OH and carboxylic groups [40]. The presence of hydrogen bond facilitates excited state hydrogen transfer. The C=O group appears at 1680 cm<sup>-1</sup>. For HL (Fig. 1(b)), the bands for NH<sub>2</sub> group at 3494 and 3390 cm<sup>-1</sup> disappear due to amidation reaction and a new broad band appears at 3458 cm<sup>-1</sup> corresponding to NH group. The more broadening due to overlap between NH, OH and carboxyl groups may causes the probability of hydrogen transfer to increase in the presence of C=O group which directly attached to NH. Absorption band at 1504 ± 5 cm<sup>-1</sup> (N=N) appears as a consequence of diazotization process (Fig. 1(c-f)). The previously discussed broad band (3458–2950 cm<sup>-1</sup>) is red shifted with more broadening. This may be attributed to extra hydrogen transfer of azo-hydrazone tautomer between N=N and *o*-NH (Scheme 3(III)). A distinguished absorption band appears related to substituent function groups attached with azo linkage. These absorption bands appears for  $\nu(\text{NO}_2)$ ,  $\nu(\text{OCH}_3)$  and  $\delta(\text{OCH}_3)$  at 1330, 2838 and 1465 cm<sup>-1</sup>, respectively.

### TGA analysis of 4-ASA, HL and HL<sub>n</sub>

The thermal behavior of 4-ASA, HL and its azo derivatives (HL<sub>n</sub>) were investigated using thermogravimetric analysis (TGA). TGA curves (Fig. 2) show that all compounds decompose in two steps in the temperature range (100–600 °C). Weight loss percentage in each stage of HL and its azo derivatives is presented in Table 2. It can be seen clearly that the mass losses obtained from the TG curves and that calculated for the corresponding molecule or molecules as well as the final decomposition product are in good agreement for all of the decomposition steps. 4-ASA TG thermogram has been previously reported by Saifullah and Rotich [19,20] showing two decomposition steps. The first one occurred in the temperature range 101–150 °C near to melting point with mass loss 30%, attributed to decarboxylation of 4-ASA [20]. The second stage (151–235 °C) is due to thermal combustion of 4-ASA [19]. Accordingly, the first stage occurred in the temperature range 170–185 °C is attributed to decarboxylation mechanism. The second stage in the temperature range 185–255 °C is mainly due to combustion of a part of the monomer (C<sub>6</sub>H<sub>4</sub>N) and at higher Temperature

Scheme 3. Possible ESPT of azo derivatives HL<sub>n</sub>.Fig. 2. The TG curves of thin films; (a) 4-ASA, (b) HL, (c) HL<sub>2</sub>, and (d) HL<sub>3</sub>.

(> 300 °C) loss acrylaldehyde molecule (C<sub>3</sub>H<sub>3</sub>O) [19]. All azo derivatives show first TG step in the temperature range ~100–250 °C losing azo part, while in the temperature region ~250–300 °C, for the second TG stage attributed to decarboxylation mechanism. At higher temperatures HL and its azo derivatives lose the acrylaldehyde molecule (C<sub>3</sub>H<sub>3</sub>O) accompanied by 4-ASA combustion.

The kinetic and thermodynamic parameters such as activation energy ( $E_a$ ), enthalpy ( $\Delta H^*$ ), entropy ( $\Delta S^*$ ) and free energy change of the decomposition ( $\Delta G^*$ ) were evaluated by applying the Coats–Redfern (CR) and Horowitz–Metzger (HM) methods [41a,b], respectively.

$$\log \left[ \frac{\log \left( \frac{W_f}{W_f - W} \right)}{T_m^2} \right] = \log \left[ \frac{AR_m}{\theta E_a} \left( 1 - \frac{2R_m T_m}{E_a} \right) \right] - \frac{E_a}{2.303 R_m T_m}, \quad (6)$$

where  $W_f$  is the mass loss at the completion of the reaction,  $W$  is the mass loss up to temperature  $T_m$ ;  $R_m$  is the gas constant,  $E_a$  is the activation energy in kJ mol<sup>-1</sup>,  $\theta$  is the heating rate and  $(1 - (2R_m T_m /$

$E_a)) \approx 1$ . A plot of the left-hand side of Eq. (6) against  $1/T$  gives a slope from which  $E_a$ , the energy of activation, was calculated, and

$$\log \left[ \log \left( \frac{W_x}{W_y} \right) \right] = \frac{\theta E_a}{2.303 R T_s^2} - \log 2.303, \quad (7)$$

where  $\theta = T - T_g$ ,  $w_y = w_x - w$ ,  $w_x$  mass loss at the completion reaction;  $w$  = mass loss up to time  $t$ . The plot of  $\log [\log (w_x/w_y)]$  vs.  $\theta$  was drawn and found to be linear from the slope ( $E_a/2.303 R T_s^2$ ) of which  $E_a$  was calculated.

The entropy of activation ( $\Delta S^*$ ), enthalpy of activation ( $\Delta H^*$ ) and the free energy change of activation ( $\Delta G^*$ ) were calculated using the following equations:

$$\Delta S^* = 2.303 \left[ \log \left( \frac{Ah}{k_B T_s} \right) \right] R, \quad (8)$$

where  $k_B$  is the Boltzmann constant,  $h$  is the Planck's constant,  $T_s$  is the peak temperature and  $A$  is the Arrhenius factor. The enthalpy of activation,  $\Delta H^*$ , and Gibbs free energy,  $\Delta G^*$ , calculated from:

$$\Delta H^* = E_a - R_m T_m \quad (9)$$

$$\Delta G^* = \Delta H^* - T_m \Delta S^* \quad (10)$$

The calculated values of  $E_a$ ,  $A$ ,  $\Delta S^*$ ,  $\Delta H^*$  and  $\Delta G^*$  for the decomposition steps are summarized in Table 3. According to obtained kinetic data, entropy was found to be positive. So, the activated compound can be thought to own less ordered structures than the reactant, while the negative values of activation entropies  $\Delta S^*$  indicate a more ordered activated compounds than the reactants and/or the reactions are slow [41c].

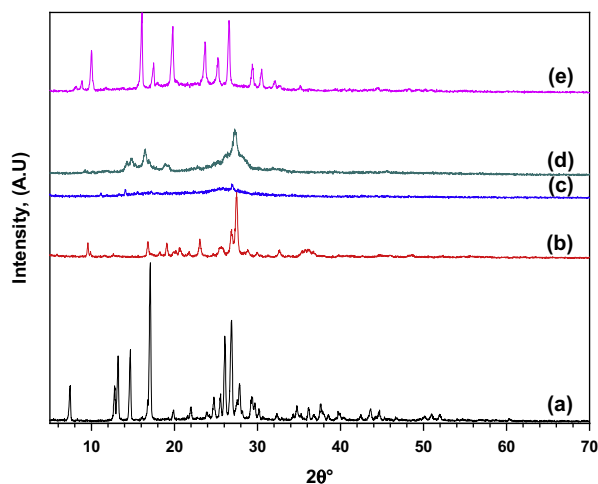
The non-spontaneous nature of the degradation reactions of the compounds were supported by the positive value of  $\Delta G^*$  in the degradation steps. The positive value of  $\Delta H^*$  at a particular temperature indicated that the process was endothermic nature. The high values of the activation energies reflect the thermal stability of the compounds. So, it is clear from TG analysis that HL more stable than its azo derivatives. Also indicate that thermal stability of HL<sub>3</sub> > HL<sub>2</sub> [42].

Table 2  
Weight loss percentage of HL and its azo derivatives (HL<sub>n</sub>).

Compound	First stage			Assignments loss of:	Second stage			Remaining Wt.% after ≈ 300 °C	
	$T_s$	Wt. loss%			$T_s$	Wt. loss%			
		Found	Calc.			Found	Calc.		
HL	170	29.9	28.0	CO <sub>2</sub> + H <sub>2</sub> O	185	43.7	43.0	C <sub>6</sub> H <sub>4</sub> N	26.4
HL <sub>2</sub>	85	39.9	39.5	C <sub>6</sub> H <sub>5</sub> N <sub>2</sub> + H <sub>2</sub> O	195	12.5	14	CO <sub>2</sub>	47.6
HL <sub>3</sub>	110	38.2	40.3	C <sub>6</sub> H <sub>4</sub> N <sub>2</sub> Cl	190	12	12.7	CO <sub>2</sub>	49.8

**Table 3**  
Kinetic and thermodynamic data of the thermal decomposition for HL and its azo derivatives (HL<sub>n</sub>).

Comp.	Decomp. step	Parameter					Parameter				
		CR method					HM method				
		$E_a$ (kJ mol <sup>-1</sup> )	$A$ (s <sup>-1</sup> )	$\Delta S^\ddagger$ (J mol <sup>-1</sup> K <sup>-1</sup> )	$\Delta H^\ddagger$ (kJ mol <sup>-1</sup> )	$\Delta G^\ddagger$ (kJ mol <sup>-1</sup> )	$E_a$ (kJ mol <sup>-1</sup> )	$A$ s <sup>-1</sup>	$\Delta S^\ddagger$ (J mol <sup>-1</sup> K <sup>-1</sup> )	$\Delta H^\ddagger$ (kJ mol <sup>-1</sup> )	$\Delta G^\ddagger$ (kJ mol <sup>-1</sup> )
HL	1st	341	$2.58 \times 10^{36}$	$4.49 \times 10^2$	337	131	344	$5.17 \times 10^{37}$	$4.74 \times 10^2$	340	123
	2nd	84.6	$2.27 \times 10^6$	$-1.28 \times 10^2$	80.3	146	94.5	$2.50 \times 10^7$	$-1.08 \times 10^2$	90.2	146
HL <sub>2</sub>	1st	69.8	$2.29 \times 10^6$	$-1.26 \times 10^2$	66.4	118	77.4	$7.60 \times 10^7$	-96.7	74.1	114
	2nd	48.7	1.49	$-2.49 \times 10^2$	42.6	226	67.4	$1.53 \times 10^2$	$-2.11 \times 10^2$	61.3	216
HL <sub>3</sub>	1st	80.6	$1.81 \times 10^7$	$-1.08 \times 10^2$	77.3	120	75.1	$9.39 \times 10^7$	-94.6	71.9	109
	2nd	43.1	$1.02 \times 10^2$	$-2.11 \times 10^2$	38.8	148	47.1	$1.96 \times 10^2$	$-2.06 \times 10^2$	42.8	149



**Fig. 3.** The XRD patterns of powder forms; (a) 4-ASA, (b) HL, (c) HL<sub>3</sub>, (d) HL<sub>4</sub>, and (e) HL<sub>2</sub>.

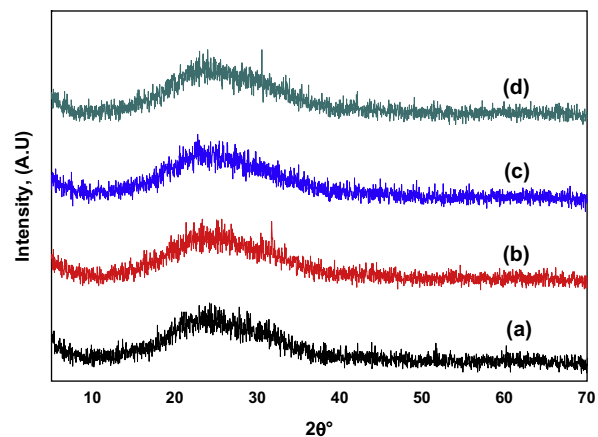


**Fig. 4.** The XRD patterns of thin film forms; (a) 4-ASA, (b) HL, (c) HL<sub>3</sub>, and (d) HL<sub>4</sub>.

#### X-ray diffraction

The X-ray diffraction patterns (XRD) of 4-ASA and its azo derivatives in powder and thin film forms are shown in Figs. 3 and 4, respectively. The XRD patterns of the powder forms indicate that all the samples are polycrystalline with different structure and various degree of crystallinity. Moreover the XRD pattern of 4-ASA (Fig. 3a) found to be, perfectly, identical to the one reported by

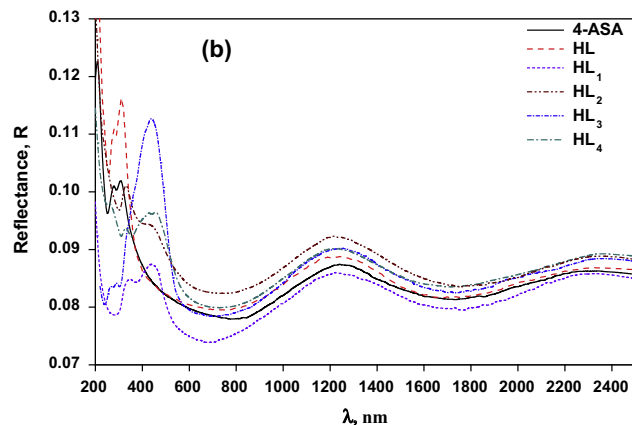
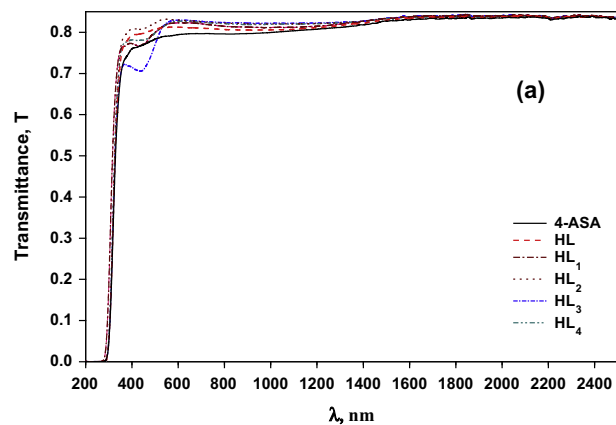


**Fig. 5.** Spectral behavior of (a) Transmittance,  $T$ , and (b) Reflectance,  $R$ , for 4-ASA, HL and HL<sub>n</sub> thin films.

Saifullah et al. and Xu et al. [19,26] and differ from 5-ASA [43]. HL is also polycrystalline structure (Fig. 3b). The XRD patterns for azo derivatives indicate a mixture of polycrystals and amorphous structure (Fig. 3c–e). The XRD patterns of thin films (Fig. 4) indicate that all thin films of 4-ASA and its derivatives are amorphous.

#### Optical properties

##### Optical constants of 4-ASA and its derivatives thin films

The absolute values of transmittance,  $T(\lambda)$ , and reflectance,  $R(\lambda)$ , for thin films of 4-ASA, HL and HL<sub>n</sub> in the wavelength range 200–2500 nm are shown in Fig. 5(a and b) respectively. There is a strong absorption in the wavelength range 200–400 nm ( $T + R < 1$ ) and very weak absorption in the wavelength range 600–2500 nm

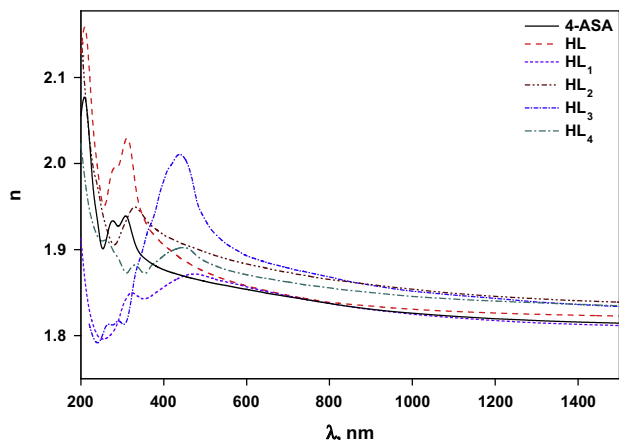


Fig. 6. Spectral behavior of refractive index,  $n$ , for 4-ASA, HL and  $HL_n$  thin films.

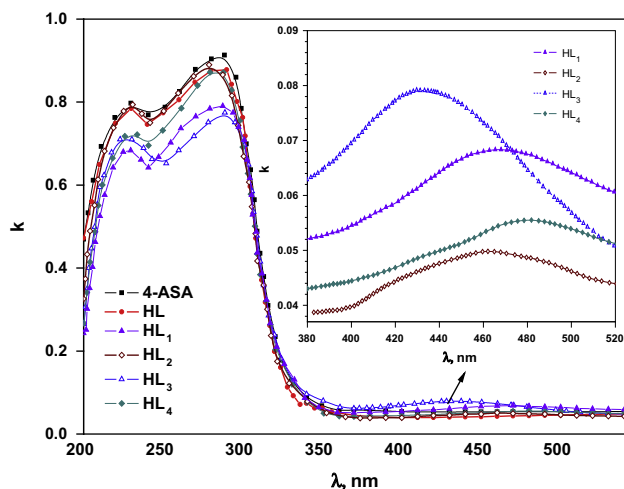


Fig. 7. Spectral behavior of absorption index,  $k$ , for 4-ASA, HL and  $HL_n$  thin films.

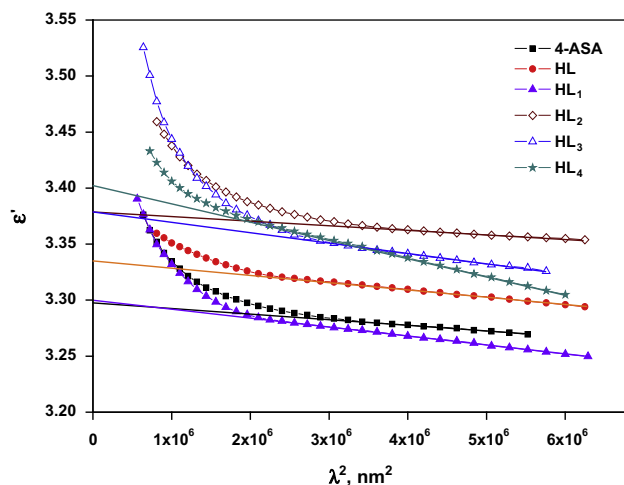


Fig. 8. Plot of  $\epsilon'$  vs.  $\lambda^2$  for 4-ASA, HL and  $HL_n$  thin films.

( $T + R \approx 1$ ). The interference appeared in the wavelength range 600–2500 nm is due to the multiple reflection which occur at the interface between film-substrate and the back reflection of the thin film [44]. The absorption phenomena in the high wavelength range can be attributed to scattering of the light [35].

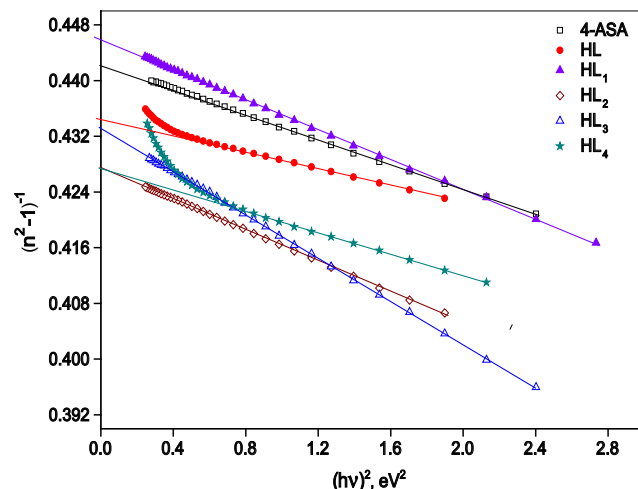


Fig. 9. Plot of  $(n^2 - 1)^{-1}$  vs.  $(h\nu)^2$  for 4-ASA, HL and  $HL_n$  thin films.

The spectral behavior of the calculated values of refractive index,  $n$ , for thin films of 4-ASA, HL and  $HL_n$  is shown in Fig. 6. The spectral behavior of  $n$  for all samples shows normal dispersion behavior at the wavelength ranged 650–2500 nm, while it shows anomalous dispersion at  $\lambda < 650$  nm. This behavior has been reported for many organic compounds [37,45]. The spectral distribution of absorption index,  $k$ , for all samples in the wavelength range 200–600 nm is shown in Fig. 7. All the materials under investigation have two peaks at 230 nm to 300 nm. Additional peak appears at the wavelength range 380–520 nm for azo derivatives only.

#### Dispersion analysis

The obtained data of refractive index,  $n$ , in the non absorbing region can be analyzed in the terms of single oscillator model to obtain the lattice dielectric constant,  $\epsilon_L$ , the carrier concentration to effective mass ratio ( $N/m^*$ ), the dispersion energy,  $E_d$ , the single oscillator energy,  $E_o$ , and the dielectric constant at infinity,  $\epsilon_\infty$ , which describes the contribution of the free carriers and the lattice vibration modes of the dispersion via the following procedure:

The real part of the dielectric constant  $\epsilon'$  ( $\epsilon' = n^2 - k^2$ ) related to the wavelength of the incident light in the non absorbing region by the following relation [37,45]:

$$\epsilon' = \epsilon_L - \frac{e^2 N}{4\pi\epsilon_0 m^* c^2} \lambda^2, \quad (11)$$

where  $e$  is the charge of the electron,  $\epsilon_0$  is the permittivity of free space and  $c$  is the velocity of light. Fig. 8 shows the relation between  $\epsilon'$  and  $\lambda^2$  in the non-absorbing region for 4-ASA and its derivatives thin films. The value of  $\epsilon_L$  can be obtained from the intersection of the extrapolation of the straight line with the  $\epsilon'$  axis, the value of  $N/m^*$  can be calculated using the slope of the straight line.

Wemple and Didomenico [46] analyzed the refractive index data below the interband absorption edge using a single oscillator equation to define the dispersion energy parameters  $E_d$  and  $E_o$  which measure the average strength of the interband optical transitions according to the relation:

$$n^2 - 1 = \frac{E_o E_d}{E_o^2 - (h\nu)^2}, \quad (12)$$

where  $h\nu$  is the energy of the incident light. Experimental verification of the above equation can be obtained by rearranging relation (12) and plotting  $(n^2 - 1)^{-1}$  vs.  $(h\nu)^2$  and fitting it to a straight line, as shown in Fig. 9. The values of  $E_o$  and  $E_d$  are determined from the

**Table 4**  
The value of the optical parameters of 4-ASA and its derivatives thin films.

Compound	$\epsilon_\infty$	$\epsilon_L$	$E_d$ (eV)	$E_o$ (eV)	$N/m^* \times 10^{54}$ ( $\text{kg}^{-1} \text{m}^{-3}$ )	$E_g$ (eV)	$E_g^*$ (eV)
4-ASA	3.26	3.30	15.54	6.88	2.10	3.60	–
HL	3.30	3.34	19.32	8.40	2.52	3.65	–
HL <sub>1</sub>	3.24	3.30	14.42	6.42	2.95	3.69	1.07
HL <sub>2</sub>	3.34	3.38	14.43	6.17	1.55	3.63	1.06
HL <sub>3</sub>	3.31	3.38	12.18	5.27	3.32	3.66	1.55
HL <sub>4</sub>	3.34	3.40	17.57	7.57	6.06	3.60	0.94

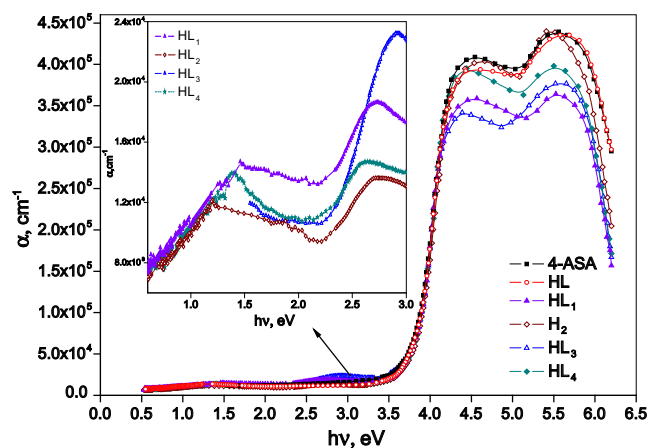


**Fig. 10.** The absorption coefficient,  $\alpha$ , as a function of the incident photon energy  $h\nu$  for 4-ASA, HL and HL<sub>n</sub> thin films.

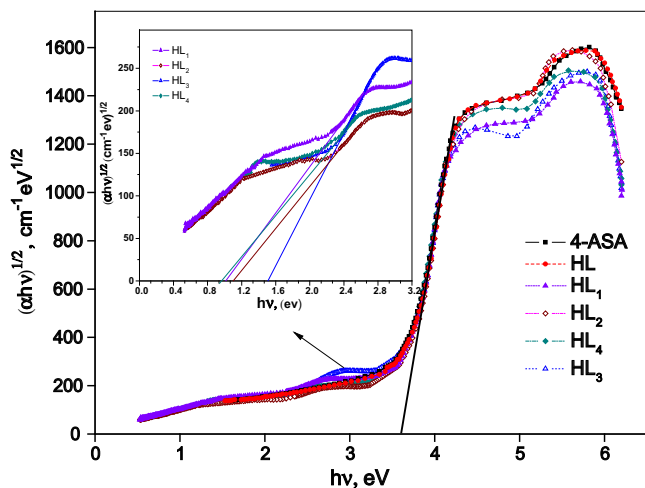


**Fig. 11.** Plot of  $(\alpha h\nu)^{1/2}$  vs.  $h\nu$  for 4-ASA, HL and HL<sub>n</sub> thin films.

slope  $(= (E_o E_d)^{-1})$  and the intersection  $(= (E_o/E_d))$  with the vertical axis. The values of  $\epsilon_\infty$  can be obtained from the intersection of the extrapolated straight line with the Y-axis when it equals  $(n_\infty^2 - 1)^{-1}$  and  $\epsilon_\infty = n_\infty^2$ . The values of  $\epsilon_L$ ,  $\epsilon_\infty$ ,  $N/m^*$ ,  $E_o$  and  $E_d$  are listed in Table 4. It is clear that,  $\epsilon_L > \epsilon_\infty$  for all compounds under study. This trend was observed for other materials [37,45] and was attributed to the contribution of a small concentration of free carriers.

#### Absorption properties of thin films

In general, the absorption spectrum gives useful information about the energy band structure of materials. The absorption

**Table 5**  
The peak position of photoluminance (PL) spectra of solutions and thin films.

Compound	Photoluminance peak position					
	Solution ( $10^{-5}$ mol/L)			Thin film		
	1	2	3	1	2	3
4-ASA	409 (P)	432 (P)	488 (Sh)	514 (P)	538 (P)	581 (Sh)
HL	407 (P)	430 (P)	490 (Sh)	512 (P)	536 (P)	579 (Sh)
HL <sub>1</sub>	–	–	–	508 (Sh)	521 (P)	579 (Sh)
HL <sub>2</sub>	–	–	–	512 (P)	522 (Sh)	580 (Sh)
HL <sub>3</sub>	–	–	–	512 (P)	522 (Sh)	580 (Sh)
HL <sub>4</sub>	–	–	–	512 (P)	522 (Sh)	580 (Sh)

coefficient,  $\alpha$ , of thin films of 4-ASA and its derivatives as a function of incident photon energy ( $h\nu$ ) is shown in Fig. 10. The absorption coefficient spectra reveal two peaks in the UV region of incident light for all compounds, and a peak in the visible region of incident light for the azo derivatives only. This behavior can be attributed to the orbital molecular transition from bonding to antibonding molecular orbitals. The band appearing at 5.55 eV is assigned to  $\pi-\pi^*$  transitions of aromatic benzene ring and the band, appearing close to the first one, located around 4.50 eV attributed to the stabilization of the higher lying  $n-\pi^*$  state by substitution. Also this state may have intramolecular charge transfer character (ICT) [27,47]. The decrease in energy gap between two bands for groups with more electron donating character (strongly donating amino group at 4-position) indicates a stronger interaction and hence a lowering of this state [27]. The bands located around 2.65–2.88 eV is assigned to  $n-\pi^*$  transitions for azodye derivatives function group  $N=N$ . The variation of the peak position can be attributed to either withdrawing or donating functional groups [48].

To determine the energy gap,  $E_g$ , and the type of optical transition responsible for optical absorption, the experimental data can be treated according to the following relation [36]:

$$\alpha h\nu = B(h\nu - E_g)^m, \quad (13)$$

where  $B$  is a constant which depends on the electronic transition probability,  $E_g$  is the optical energy gap of the material,  $m$  is the power which characterizes the transition process, where  $m = 1/2$  and  $3/2$  for direct allowed and forbidden transitions, respectively, and  $m = 2$  and  $3$  for indirect allowed and forbidden transitions, respectively. The best fit for our data which are shown in Fig. 11, ensuring the occurrence of indirect allowed transition. The fundamental energy gap  $E_g$  and the onset energy gap  $E_g^*$  for 4-ASA and its derivatives are tabulated in Table 4. The onset  $E_g^*$  appears only for the azodye derivatives. The variation of the values of  $E_g^*$  can be attributed to either withdrawing or donating functional groups. It is those fundamental optical energy gaps  $E_g$  nearly have the same values (3.60–3.69) eV. The onset energy gaps have values in the range 0.94–1.55 eV depending on the substituent group.

#### Emission properties

The photoluminescence (PL) spectra of 4-ASA and its derivatives as solution and thin film forms are investigated. A comparison

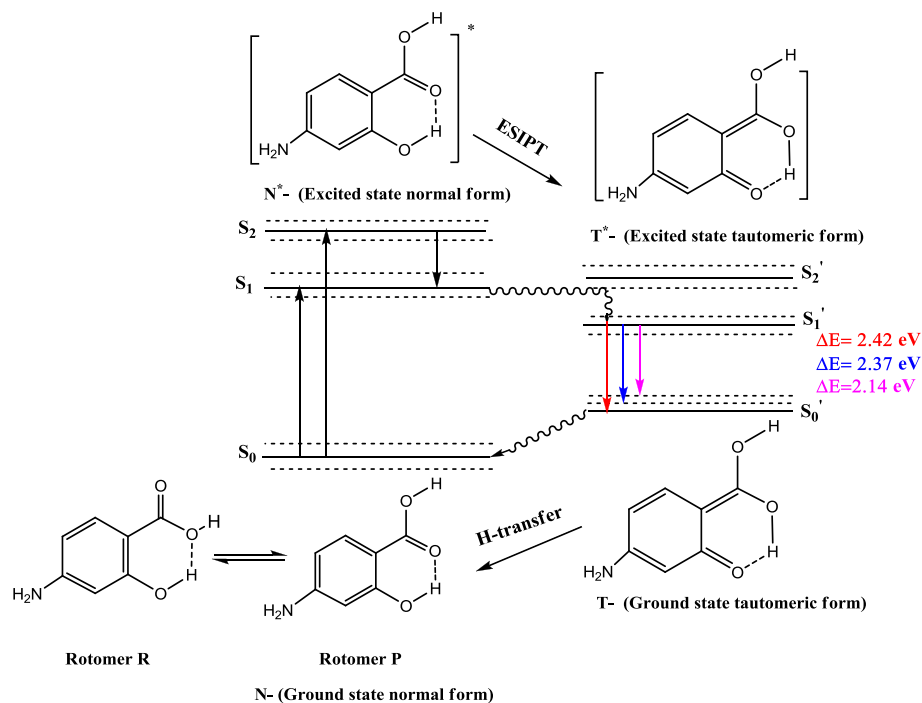
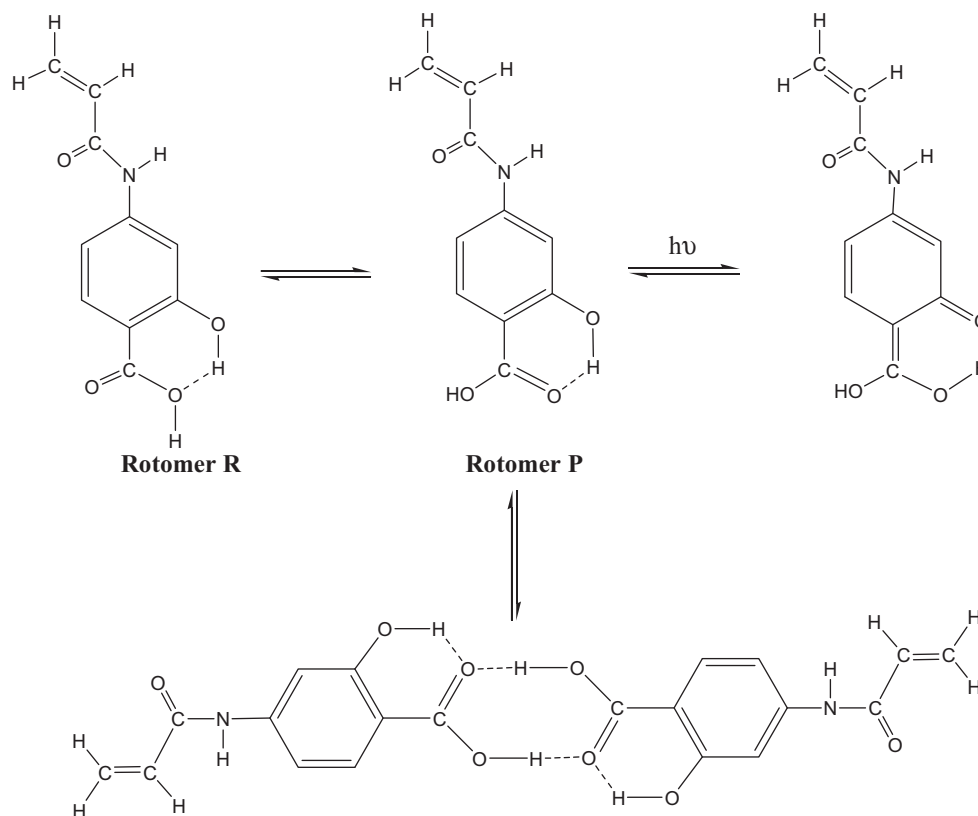


Fig. 12. Excited state intramolecular proton transfer (ESIPT) pathway of 4-ASA at  $\lambda_{\text{max}} = 365$  nm.



Scheme 4. Intra- and inter-molecular hydrogen bond of HL.

between PL spectra of solution ( $10^{-5}$  mol/L, using methanol as a solvent) and thin films are presented in Table 5. No significant emission peaks for the solution of azodye derivatives, while all the thin films samples of 4-ASA and its derivatives have PL spectra.

The PL spectra for thin films of 4-ASA and HL have the same behavior as that of the solutions, but with red shift. This shift can be attributed to the effect of solvent [49]. The PL spectra of 4-ASA, HL and  $HL_n$  thin films are shown in Fig. 12. The photoluminescence

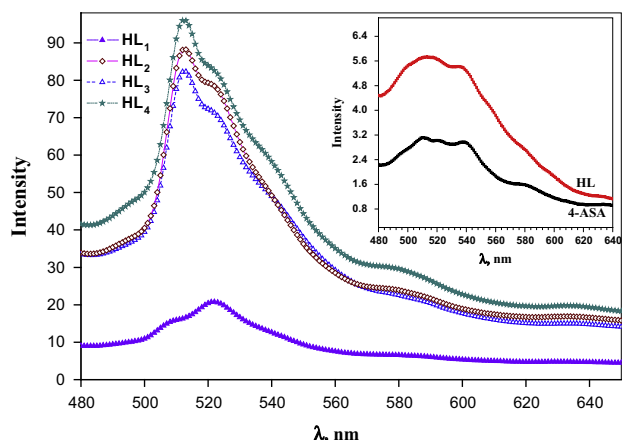


Fig. 13. Emission spectra for 4-ASA, HL and  $HL_n$  thin films.

phenomena (PL) which appear for thin films of 4-ASA and its derivatives show three main emission transitions at 512, 530 and 580 nm.

The possible excited intramolecular proton transfer pathway of 4-ASA and its derivatives at  $\lambda_{\max} = 365$  nm are shown in Fig. 12. 4-ASA (P-form) undergoes ESIPT. 4-ASA has short lifetime, and low quantum yield which attributed to stabilization of the  $S_2$  state of  $n-\pi^*$  indicating an increased deactivation [27]. Emission fluorescence bands could be observed as the absorption is from  $N$  to  $N^*$  ( $N^*$  is excited state normal form) and the emission is from  $T^*$  to  $T$  ( $T^*$  is excited state tautomeric form).

The amidation process slightly enhances the fluorescence spectrum due to direct attachment of amino group with carbonyl group, which decrease donation of amino to phenyl ring. Intra- and inter-molecular hydrogen bond transfer of HL is shown in Scheme 4. It seems that HL easily undergoes ESIPT with rotomer  $P$ . Also it can formed dimer structure through intermolecular hydrogen bond between two molecules.

Diazotization reaction clearly enhances the PL intensity (Fig. 13). This may be due to the presence of electron density at *para* position with respect to the phenolic OH group which exhibit preference tautomer which undergoes ESIPT [27]. Also, azo moiety can undergo another ESIPT as confirmed by IR spectra of azo derivatives of 4-ASA through intramolecular hydrogen bond [24]. The NH group playing the role of planar acceptors joined by azo ( $-N=N-$ ) group. According to Scheme 3,  $HL_n$  undergo fast intramolecular proton transfer between the enol azo form (I) and the keto hydrazone form (III), in which the excited transition state will evolve six membered ring [21–23]. Therefore, the system has two photoisomerisable units capable of undergoing a double ESIPT process (Scheme 3(II and III)).

## Conclusion

In the present work, we discussed the effect of amidation and diazotization reactions on the optical and thermal properties of 4-ASA. 4-ASA and its derivatives are polycrystalline in the powder form and amorphous in the thin film form. Investigation of thermal properties is performed using thermogravimetric analysis (TGA). All the thermal parameters such as activation energy ( $E_a$ ), enthalpy ( $\Delta H^*$ ), entropy ( $\Delta S^*$ ) and free energy change of the decomposition ( $\Delta G^*$ ) are affected by amidation and diazotization processes. The spectral behavior of  $n$  shows anomalous dispersion in the wavelength range 200–650 nm and normal dispersion in the wavelength range 650–2500 nm. The single oscillator model in the non-absorbing region of spectra revealed values of  $\epsilon_\infty$  in the range 3.24–3.34 and  $\epsilon_L$  in the range 3.30–3.40. Generally,  $\epsilon_L$  was found to

be lower than  $\epsilon_\infty$  for all compounds which indicate the existence of free carriers. The optical transition are found to be indirect allowed with values energy gap,  $E_g$ , of 3.60–3.69 eV for fundamental optical transition and onset energy gap  $E_g^*$ , of 0.94–1.55 eV for azo derivatives only. All of the 4-ASA and its derivatives revealed emission spectra in the wavelength rang 500–600 nm. Diazotization remarkably enhances the PL spectra, due to the presence of an extra ESIPT.

## References

- [1] H.E. Fierz-David, L. Blangey, *Fundam. Process. Dye Chem.* (1949).
- [2] G.G. Alfonso, J.L.G. Ariza, *Microchem. J.* 26 (1981) 574–585.
- [3] N. Charton, A. Feldermann, A. Theis, M.H. Stenzel, T.P. Davis, C.B. Kowolik, *J. Polym. Sci. Part A: Polym. Chem.* 42 (2004) 5170–5179.
- [4] B. Ray, B.M. Mandal, *J. Polym. Sci. Part A: Polym. Chem.* 37 (1999) 493–499.
- [5] M.K. Chourasia, S.K. Jain, *J. Pharm. Pharmaceut. Sci.* 6 (2003) 33–66.
- [6] M. Mahkam, L. Doostie, S.O.R. Siadat, *InflammoPharmacology* 14 (2006) 72–75.
- [7] Y.J. Jung, J.S. Lee, Y.M. Kim, *J. Pharm. Sci.* 89 (2000) 594–602.
- [8] (a) F. Qiu, Y. Cao, H. Xu, Y. Jiang, Y. Zhou, *J. Liu, Dyes Pigm.* 75 (2007) 454–459; (b) I.S.K. Yesodha, C.K.S. Pillai, N. Tsutsumi, *Prog. Polym. Sci.* 29 (2004) 45–74.
- [9] D. Kanis, M. Ratner, T. Marks, *Chem. Rev.* 94 (1994) 195–242.
- [10] (a) V.K. Bhardwaj, N. Singh, M.S. Hundal, *Tetrahedron* 62 (2006) 7878–7886; (b) N. DiCesare, J.R. Lakowicz, *Org. Lett.* 3 (2001) 3891–3893.
- [11] (a) S. Ghosh, A. Banthia, Z. Chen, *Tetrahedron* 61 (2005) 2889–2896; (b) I.A. Harvey, A. Abell, *Tetrahedron* 56 (2000) 9763–9771.
- [12] (a) W.M.F. Fabian, L. Antonov, D. Nedeltcheva, F.S. Kamounah, P.J.J. Taylor, *Phys. Chem. A* 108 (2004) 7603–7612; (b) S. Pieraccini, G. Gottarelli, R. Labruto, S. Masiero, O. Pandoli, G. Spada, *Chem. Eur. J.* 10 (2004) 5632–5639; (c) F.R. Van der Zee, F.J. Cervantes, *Biotechnol. Adv.* 27 (2009) 256–277; (d) Y.G. Hong, J.D. Gu, *Appl. Microbiol. Biotechnol.* 88 (2010) 637–643.
- [13] R.H. Böger, S.M. Bode-Böger, F.M. Gutzki, D. Tsikas, H.P. Weskott, J.C. Frölich, *Clin. Sci.* 84 (1993) 517–524.
- [14] M.F. Attie, J.J.R. Gill, J.L. Stock, A.M. Spiegel, J.R.W. Downs, M.A. Levine, S.J. Marx, *J. Clin. Invest.* 72 (1983) 667–676.
- [15] M.J. Landsman, J.E. Mancuso, S.P. Abramow, *Clin. Podiat. Med. Surg.* 13 (1996) 55–71.
- [16] Y. Kawashima, M. Okumura, H. Takenaka, *Science* 216 (1982) 1127–1128.
- [17] Z.B. Zhao, H.X. Zheng, Y.G. Wei, J. Liu, *Synthesis of azo derivatives of 4-aminosalicylic acid*, *Chin. Chem. Lett.* 18 (2007) 639–642.
- [18] S.F. Sheng, H.X. Zheng, J. Liu, Z.B. Zhao, *Chin. Chem. Lett.* 19 (2008) 419–422.
- [19] B. Saifullah, M.Z. Hussein, S.H. Hussein-Ali, P. Arulsevan, S. Fakurazi, *Chem. Cent. J.* 7 (2013) 72.
- [20] M.K. Rotich, B.D. Glass, M.E. Brown, *J. Therm. Anal. Calorim.* 64 (2001) 681–688.
- [21] G.A. Ibanéz, A.C. Olivieri, G.M. Escandar, *J. Chem. Soc. Faraday* 93 (1997) 543–551.
- [22] G.N. Ledesma, G.A. Ibanéz, G.M. Escandar, A.C. Olivieri, *J. Mol. Struct.* 415 (1997) 115–121.
- [23] G.A. Ibanéz, A.C. Olivieri, G.M. Escandar, *J. Mol. Struct.* 435 (1997) 199–206.
- [24] J. Chen, Z. Yin, *Dyes Pigm.* 102 (2014) 94–99.
- [25] P. Rochon, J. Gosselin, A. Natansohn, S. Xie, *Appl. Phys. Lett.* 60 (1992) 4–5.
- [26] D. Xu, M. Zhao, J. Ren, G. Li, Z. Liao, *Food Res. Int.* 43 (2010) 2077–2080.
- [27] H.C. Joshi, C. Gooijer, G. van der Zwan, *J. Fluoresc.* 13 (2003) 227–234.
- [28] K. Suyal, N.K. Joshi, R. Rautela, H.C. Joshi, S. Pant, *J. Photochem. Photobiol. A: Chem.* 216 (2010) 51–58.
- [29] A.A. El-Bindary, A.Z. El-Sonbati, M.A. Diab, M.E. Attallah, *Spectrochim. Acta A* 86 (2012) 547–553.
- [30] A.Z. El-Sonbati, A.A. El-Bindary, R.M. Issa, H.M. Kera, *Des. Mon. Polym.* 7 (2004) 445–459.
- [31] A.Z. El-Sonbati, A.A. El-Bindary, M.A. Diab, M.A. El-Ela, S.A. Mazrouh, *Polym. Deg. Stab.* 42 (1993) 1–11.
- [32] A.Z. El-Sonbati, A.A. El-Bindary, M.A. Diab, M.A. El-Ela, S.A. Mazrouh, *Polymer* 35 (1994) 647–652.
- [33] A.Z. El-Sonbati, A.A. El-Bindary, I.G. Rashed, *Spectrochim. Acta A* 58 (2002) 1411–1424.
- [34] M.A. Diab, A.Z. El-Sonbati, A.A. El-Bindary, M.Z. Balboula, *J. Mol. Struct.* 1040 (2013) 171–179.
- [35] H.M. Zeyada, M.M. EL-Nahass, I.S. Elashmawi, A.A. Habashi, *J. Non-Crystalline Solids* 358 (2012) 625–636.
- [36] E.M. El-Menyawy, N.A. El-Ghamaz, H.H. Nawar, *J. Mol. Struct.* 1036 (2013) 144–150.
- [37] N.A. El-Ghamaz, A.Z. El-Sonbati, M.A. Diab, A.A. El-Bindary, H.A. Seyam, *Solid State Sci.* 19 (2013) 19–26.
- [38] M.M. El-Nahass, S. Yagmour, *Appl. Surface Sci.* 255 (2008) 1631–1636.
- [39] M.M. El-Nahass, A.F. El-Deeb, H.S. Metwally, H.E.A. El-sayed, A.M. Hassanien, *Solid State Sci.* 12 (2010) 552–557.
- [40] M. Takahashi, Y. Ishikawa, H. Ito, *Chem. Phys. Lett.* 531 (2012) 98–104.
- [41] (a) A.W. Coats, J.P. Redfern, *Nature* 20 (1964) 68–69; (b) H.W. Horowitz, G. Metzger, *Anal. Chem.* 35 (1963) 1464–1468; (c) S. Alghool, H.F.A. El-Halim, A. Dahshan, *J. Mol. Struct.* 983 (2010) 32–38.

- [42] N.A. El-Ghamaz, A.Z. El-Sonbati, M.A. Diab, A.A. El-Bindary, M.K. Awad, Sh.M. Morgan, *Mater. Sci. Semicond. Process.* 19 (2014) 150–162.
- [43] D. Hu, L. Liu, W. Chen, S. Li, Y. Zhao, *Int. J. Mol. Sci.* 13 (2012) 6454–6468.
- [44] Y. Laaziz, A. Bennouna, N. Chahboun, A. Outzourhit, E.L. Ameziane, *Thin Solid Films* 372 (2000) 149–155.
- [45] (a) N.A. El-Ghamaz, H.M. El-Mallah, A.Z. El-Sonbati, M.A. Diab, A.A. El-Bindary, A.M. Barakat, *Solid State Sci.* 22 (2013) 56–64;
- (b) H.M. El-Mallah, N.A. El-Ghamaz, M.A. Waly, *J. Phys. D* 43 (2010). 455407–45515.
- [46] S.H. Wemple, M. Didomenico, *Phys. Rev. B* 3 (1971) 1338–1351.
- [47] Y. Kim, M. Yoon, *Bull. Korean Chem. Soc.* 19 (1998) 980–985.
- [48] N.A. El-Ghamaz, A.Z. El-Sonbati, Sh.M. Morgan, *Mol. Struct.* 1027 (2012) 92–98.
- [49] J.H. Hsu, W. Fann, P.H. Tsao, K.R. Chuang, S.A. Chen, *J. Phys. Chem. A* 103 (1999) 2375–2380.